Multi-Level Acceleration of Parallel Coupled Partitioned Fluid-Structure Interaction with Manifold Mapping

D.S. Blom, B. Uekermann, M. Mehl, A.H. van Zuijlen, and H. Bijl

Abstract Strongly coupled fluid-structure interaction simulations often suffer from slow convergence, limited parallel scalability or difficulties in using black-box solvers. As partitioned simulations still play an important role in cases where new combinations of models, discretizations and codes have to be tested in an easy and fast way, we propose a combination of a parallel black-box coupling with a manifold mapping algorithm as an acceleration method. In this approach, we combine a computationally inexpensive low-fidelity FSI model with a high-fidelity FSI model to reduce the number of coupling iterations of the high fidelity FSI model. Information from previous time steps is taken into account with a secant update step similar to the Broyden update. The used black-box approach is applied for an incompressible laminar flow over a fixed cylinder with an attached flexible flap and a wave propagation in a three-dimensional elastic tube problem. A reduction of approximately 55 % in terms of high fidelity iterations is achieved compared to the Anderson mixing method if the fluid and the structure solvers are executed in parallel.

D.S. Blom (✉) • A.H. van Zuijlen • H. Bijl
Faculty of Aerospace Engineering, Delft University of Technology, P.O. Box 5058, 2600 GB Delft, The Netherlands
e-mail: d.s.blom@tudelft.nl; a.h.vanzuijlen@tudelft.nl

B. Uekermann
Department of Computer Science, Technische Universität München, Boltzmannstraße 3, Garching, Germany
e-mail: uekerman@in.tum.de

M. Mehl
Universität Stuttgart, Universitätsstraße 38, Stuttgart, Germany
e-mail: miriam.mehl@ipvs.uni-stuttgart.de

M. Mehl et al. (eds.), *Recent Trends in Computational Engineering - CE2014*,
Lecture Notes in Computational Science and Engineering 105,
DOI 10.1007/978-3-319-22997-3_8

1 Introduction

Multi-physics involves multiple simultaneous physical phenomena. Fluid-structure interaction (FSI) is an example where multiple physical models are coupled [9]. Examples where FSI is apparent are aero-elasticity [25], arterial flow [15] and airbag deployment [35]. Also, the deployment of parachute systems [41] can be modelled with strongly coupled FSI solvers. The simulations need to be performed within a reasonable time frame, thus giving the need for an efficiency improvement of FSI solvers.

Highly sophisticated software codes are available for each single physical phenomena. It is desirable to reuse these codes for multi-physics simulations including FSI problems where separate fluid and structure solvers need to be coupled. This partitioned approach [26] is in contrast to the monolithic approach [7, 29, 42] where all governing equations are implemented in a single software package and solved as a large system of equations. Besides the partitioned and monolithic approach, different mixed forms have been proposed such as splitting methods [3], which separate the fluid-structure system in a fluid velocity part and a pressure-structure part. Discretization information needs to be available for such approaches, a fact that excludes commercial packages in general. This is also a drawback for methods that utilize the exact Jacobian [39].

A large number of coupling schemes that only consider input/output information of the fluid and structure solvers are already available in literature, such as Aitken's method [33], vector extrapolation [34], interface-GMRES(R) [37, 38], and the interface quasi-Newton inverse least squares (IQN-ILS) technique [15, 19]. The IQN-ILS technique [19] is an efficient [15, 16] and robust black-box coupling algorithm for which convergence theorems are available in [30]. The IQN-ILS algorithm is mathematically equivalent to the Anderson mixing method [1, 28, 47] which can be categorized as a multisecant method as discussed by Fang and Saad [24]. When applied to linear problems, it can be shown that the Anderson mixing method is essentially equivalent to the GMRES method [47], which has also been shown for the IQN-ILS method [31]. An overview of several partitioned coupling techniques applicable to FSI can be found in [2, 45]. Many classical coupling approaches are based on a sequential execution of the fluid and structure solver, which might hinder the parallel performance for off-balanced problems. This is the standard case with an expensive flow problem coupled to a cheap structure problem. In [36, 44], we studied the performance of several classical schemes applied to a parallel execution of both physical solvers. Here, the IQN-ILS technique showed encouraging results.

Nevertheless, an implication of only using input and output information of the fluid and structure solver is that still a too large number of sub-iterations is necessary to obtain a strongly coupled solution. This means that both solvers are called multiple times per time step. A promising idea is to combine an inexpensive low-fidelity model with a full high-fidelity model to perform a large amount of sub-iterations with the low fidelity model only [40]. The question remains how to

efficiently couple the multi-fidelity models. Van Zuijlen and Bijl [46] developed a multi-level acceleration technique, which is based on the assumption that the flow solver provides a geometric multigrid solver. Coarse and fine level sub-iterations are used alternately, resulting in substantial gains in computational costs. This technique hinges on the availability of a geometric multigrid solver for the fluid domain, which poses problems if black-box solvers are considered. In [17], the multi-level IQN-ILS algorithm is presented which shows the potential of a multi-level acceleration framework for FSI where the fluid and structure solvers are considered as black boxes. A coarse grid is used as a low-fidelity model in order to build an approximate Jacobian, which is reused by the finer grids to accelerate the convergence of the IQN-ILS algorithm.

Originating from multi-fidelity optimization, the aggressive space mapping algorithm has been used in [40] to efficiently couple a high-fidelity model with a low-fidelity model for a FSI problem. Scholcz et al. [40] consider the FSI interface problem as an optimization problem. Bandler proposed the original space mapping algorithm in [4] for modeling and design of engineering devices and systems. Thereafter, the aggressive space mapping approach [5] was introduced based on a quasi-Newton iteration that utilizes each fine model iterate as soon as it is available. The basis of the space mapping algorithm is the parameter extraction step which establishes the mapping and updates the surrogate. However, breakdown of the algorithm may occur due to non-uniqueness of the parameter extraction step [6]. Output space mapping [32] aims at reducing the misalignment between the coarse and fine models by adding the difference between the two to the response of the coarse model. An overview of different space mapping algorithms in given in [6].

In [10, 11], the use of manifold mapping [23] is investigated in order to solve the partitioned FSI problem. Manifold mapping has proven to be an efficient algorithm resulting in less high-fidelity iterations compared to aggressive space mapping [23] and output space mapping [20]. In this contribution, we combine the ideas of Mehl et al. [36], Uekermann et al. [44], and [10, 11]: we study the manifold mapping when used for the parallel FSI system. Special focus is given on the comparison to the serial system as well as to classical approaches.

The paper is structured as follows: the FSI problem is introduced in Sect. 2, Sect. 3 introduces the manifold mapping algorithm. The application of the manifold mapping technique is shown in Sect. 4 for several test cases. The paper is concluded in Sect. 5.

2 Fluid-Structure Interaction

The fluid-structure interaction (FSI) problem is partitioned into a fluid domain and a structure domain. The separate domains are coupled on the fluid-structure interface through the interface conditions consisting of the kinematic and the dynamic boundary conditions.

The fluid solver and the structure solver are considered as black boxes. In other words, only the input and output information is accessible. Whether a compressible or incompressible, viscous or inviscid flow is considered does not influence the used methodology described in this paper. Also, different models for the structure domain can be applied, since only the input and output information from the fluid solver and structure solver is considered to be accessible.

Therefore, at each time step the response of the fluid solver F_f is defined as

$$\mathbf{y} = F_f(\mathbf{x}), \tag{1}$$

where $\mathbf{x}$ denotes the displacement of the fluid-structure interface and $\mathbf{y}$ denotes the force acting on the fluid-structure interface. The response of the structure solver F_s is consequently defined as

$$\mathbf{x} = F_s(\mathbf{y}). \tag{2}$$

For a sequential execution of both solvers, the fixed point equation

$$\mathbf{x} = F_s \circ F_f(\mathbf{x}) \tag{3}$$

must be satisfied at every time step. This can also be written as the interface residual

$$\mathbf{R}(\mathbf{x}) = F_s \circ F_f(\mathbf{x}) - \mathbf{x}. \tag{4}$$

For a parallel execution of both solvers, the fixed point equation

$$\begin{pmatrix} 0 & 1 \\ 1 & 0 \end{pmatrix} \begin{pmatrix} F_f(\mathbf{x}) \\ F_s(\mathbf{y}) \end{pmatrix} = \begin{pmatrix} \mathbf{x} \\ \mathbf{y} \end{pmatrix}. \tag{5}$$

needs to be satisfied, which corresponds to the residual definition:

$$\mathbf{R}\begin{pmatrix} \mathbf{x} \\ \mathbf{y} \end{pmatrix} = \begin{pmatrix} F_s(\mathbf{y}) - \mathbf{x} \\ F_f(\mathbf{x}) - \mathbf{y} \end{pmatrix}. \tag{6}$$

For the sake of reusing the same notation for both cases, sequential and parallel execution, we also refer to the last definition as $\mathbf{R}(\mathbf{x})$. In this case, $\mathbf{x}$ consists of both, displacement and force values.

3 Manifold Mapping

Manifold mapping is a surrogate-based optimization technique, i.e., the quality of the initial solution or approximation of the low-fidelity model is iteratively improved. The goal of a surrogate-based optimization technique is to decrease the

computational time of the optimization process. Here, a fluid-structure interaction simulation is considered for which the coupling represents the optimization problem.

In the following subsection, the basic terminology is introduced and the manifold mapping is explained. The reader is referred to Echeverría and Hemker [22] for the theoretical basis of the technique.

3.1 Manifold Mapping Terminology

Two types of models are distinguished: a fine model and a coarse model. It is assumed that the fine model is accurate, but requires a high computational cost to evaluate. The coarse model, on the contrary, is considered to be computationally less costly, but also less accurate in comparison to the fine model.

3.1.1 The Fine Model

The fine model response is denoted by $\mathbf{f} : X \subset \mathbb{R}^n \rightarrow \mathbb{R}^n$, where $\mathbf{x} \in X$ represents the control variable of the optimization problem. The fine model cost function is defined as $\mathscr{F}(\mathbf{x}) = ||\mathbf{f}(\mathbf{x}) - \mathbf{q}||$, which represents the discrepancy between the design specification $\mathbf{q} \in \mathbb{R}^n$ and a particular response of the model $\mathbf{f}(\mathbf{x})$. Therefore, a minimization problem needs to be solved:

$$\mathbf{x}_f^\star = \arg\min_{\mathbf{x} \in X} ||\mathbf{f}(\mathbf{x}) - \mathbf{q}|| . \tag{7}$$

When the manifold mapping technique is applied to the fluid-structure interaction problem, the fine model response is defined as the interface residual $\mathbf{f}(\mathbf{x}) := \mathbf{R}(\mathbf{x})$, (4) or (6), whereas $\mathbf{q}$ is then set to 0 ($\in \mathbb{R}^n$).

3.1.2 The Coarse Model

The coarse model response is denoted by $\mathbf{c}^z : Z \subset \mathbb{R}^m \rightarrow \mathbb{R}^m$, where $\mathbf{z} \in Z$ represents the control variable of the coarse model. The coarse model cost function is defined as $\mathscr{C}(\mathbf{x}) = \left|\left|\mathbf{p}^{-1}\left(\mathbf{c}^z\left(\mathbf{p}\left(\mathbf{x}\right)\right)\right) - \mathbf{q}_k\right|\right|$, with the mapping $\mathbf{p} : X \rightarrow Z$, and the inverse of the mapping $\mathbf{p}^{-1} : Z \rightarrow X$. $\mathbf{p}$ can be interpreted as a mapping from the fine model design space to the coarse model design space. The design specification $\mathbf{q}_k \in \mathbb{R}^n$ of the coarse model is iteratively updated during the minimization process of the fine model. k represents the iteration counter of the manifold mapping algorithm. Therefore, the optimization of the coarse model is defined as

$$\mathbf{x}_c^\star = \arg\min_{\mathbf{x} \in X} \left|\left|\mathbf{p}^{-1}\left(\mathbf{c}^z\left(\mathbf{p}\left(\mathbf{x}\right)\right)\right) - \mathbf{q}_k\right|\right| . \tag{8}$$

Radial basis function interpolation is used for the mapping $\mathbf{p}$ between the fine model design space X and the coarse model design space Z. In the remainder of this work, the coarse model response is denoted by $\mathbf{c}$

$$\mathbf{c}(\mathbf{x}) = \mathbf{p}^{-1}\left(\mathbf{c}^{z}(\mathbf{p}(\mathbf{x}))\right). \tag{9}$$

This means, the mapping $\mathbf{p}$ and the inverse mapping $\mathbf{p}^{-1}$ are implicitly assumed for simplicity, and are not included in the formulations.

3.2 Manifold Mapping Algorithm

The manifold mapping algorithm, as proposed in [21], introduces the mapping $\mathbf{S}$: $\mathbf{c}(X) \rightarrow \mathbf{f}(X)$ with the goal to correct for the misalignment between the fine and coarse model. With the mapping $\mathbf{S}$, the response $\mathbf{c}(\mathbf{x}_f^{\star})$ is mapped to $\mathbf{f}(\mathbf{x}_f^{\star})$ and the tangent plane for $\mathbf{c}(X)$ at $\mathbf{c}(\mathbf{x}_f^{\star})$ is mapped to the tangent plane for $\mathbf{f}(X)$ at $\mathbf{f}(\mathbf{x}_f^{\star})$. $\mathbf{S}$ is defined as the affine mapping

$$\mathbf{S}\left(\mathbf{c}(\mathbf{x})\right) = \mathbf{f}\left(\mathbf{x}_f{}^{\star}\right) + \bar{S}\left(\mathbf{c}(\mathbf{x}) - \mathbf{c}\left(\mathbf{x}_f{}^{\star}\right)\right) \tag{10}$$

for an unknown solution $\mathbf{x}_f{}^{\star}$ and with $\bar{S}$ specified as

$$\bar{S} = \mathbf{J}_f\left(\mathbf{x}_f\right)\mathbf{J}_c{}^{\dagger}\left(\mathbf{x}_f\right). \tag{11}$$

The Jacobian of the fine model $\mathbf{J}_f$ and the Jacobian of the coarse model $\mathbf{J}_c$ are, however, assumed to be unavailable for a black-box fluid-structure interaction problem and will be approximated. The symbol † indicates the pseudo-inverse. Now, each manifold mapping iterate is defined by a coarse model optimization:

$$\mathbf{x}_{k+1} = \arg\min_{\mathbf{x}\in X} \left|\left|\mathbf{c}(\mathbf{x}) - \mathbf{c}(\mathbf{x}_k) + \bar{S}^{\dagger}\left(\mathbf{f}(\mathbf{x}_k) - \mathbf{q}\right)\right|\right|, \tag{12}$$

where the pseudo-inverse of the manifold mapping function $\bar{S}^{\dagger}$ is approximated by a sequence T_k, resulting in

$$\mathbf{x}_{k+1} = \arg\min_{\mathbf{x}\in X} ||\mathbf{c}(\mathbf{x}) - \mathbf{q}_k|| \quad \text{with} \quad \mathbf{q}_k = \mathbf{c}(\mathbf{x}_k) - T_k\left(\mathbf{f}(\mathbf{x}_k) - \mathbf{q}\right). \tag{13}$$

The approximation of the pseudo-inverse of the manifold mapping function T_k requires the singular value decomposition of the matrices ΔC_k and ΔF_k at each iteration k. The columns of ΔC_k and ΔF_k span the coarse and fine model tangent space at the current iteration as in

$$\Delta F_k = \left[\mathbf{f}(\mathbf{x}_{k+1}) - \mathbf{f}(\mathbf{x}_k), \cdots, \mathbf{f}(\mathbf{x}_{k+1}) - \mathbf{f}\left(\mathbf{x}_{\max(k+1-n,0)}\right)\right] \tag{14}$$

and

$$\Delta C_k = \left[\mathbf{c}\left(\mathbf{x}_{k+1}\right) - \mathbf{c}\left(\mathbf{x}_k\right), \cdots, \mathbf{c}\left(\mathbf{x}_{k+1}\right) - \mathbf{c}\left(\mathbf{x}_{\max(k+1-n,0)}\right)\right]. \tag{15}$$

The singular value decomposition's of ΔC and ΔF are defined as:

$$\Delta C_k = U_c \, \Sigma_c \, V_c^T \quad \text{and} \quad \Delta F_k = U_f \, \Sigma_f \, V_f^T. \tag{16}$$

The design specification $\mathbf{q}_k$ is updated at each iteration k with T_k given by

$$T_k = \Delta C_k \, \Delta F_k{}^{\dagger} + \left(I - U_c \, U_c{}^T\right)\left(I - U_f \, U_f{}^T\right) \tag{17}$$

[21]. The manifold mapping procedure is started with an extrapolation step of the solutions of the previous time steps in order to initialize the algorithm with a good initial guess. The resulting algorithm is shown in Fig. 1.

Generally, the number of degrees of freedom n on the fluid-structure interface is much larger than the number of columns of ΔC_k and ΔF_k. Therefore, the computational cost of the manifold mapping technique is limited. It mainly consists of the singular value decomposition of two $n \times k$ matrices. In order to reduce the number of fine model evaluations per time step, the matrices ΔC_k and ΔF_k can be combined with the information from r previous time steps, as in the IQN-ILS(r) approach [19]:

$$\Delta F = \left[\Delta F^{u+1} \;\; \Delta F^{u} \;\; \ldots \;\; \Delta F^{u-r+2} \;\; \Delta F^{u-r+1}\right] \tag{18}$$

$$\Delta C = \left[\Delta C^{u+1} \;\; \Delta C^{u} \;\; \ldots \;\; \Delta C^{u-r+2} \;\; \Delta C^{u-r+1}\right], \tag{19}$$

with $u + 1$ marking the recent time step. The notation MM(r) indicates that information from r time steps is reused. When information from previous time steps

$\mathbf{x_0}^{u+1} = \frac{5}{2}\mathbf{x}^u - 2\mathbf{x}^{u-1} + \frac{1}{2}\mathbf{x}^{u-2}$
$T_0 = I$
for $k = 0 \rightarrow k_{max}$ **do**
  $\mathbf{q}_k = \mathbf{c}\left(\mathbf{x}_k\right) - T_k\left(\mathbf{f}\left(\mathbf{x}_k\right) - \mathbf{q}\right)$
  $\mathbf{x}_{k+1} = \arg\min_{\mathbf{x} \in X} ||\mathbf{c}\left(\mathbf{x}\right) - \mathbf{q}_k||$
  $\Delta F = \left[\mathbf{f}\left(\mathbf{x}_{k+1}\right) - \mathbf{f}\left(\mathbf{x}_k\right), \cdots, \mathbf{f}\left(\mathbf{x}_{k+1}\right) - \mathbf{f}\left(\mathbf{x}_{\max(k+1-n,0)}\right)\right]$
  $\Delta C = \left[\mathbf{c}\left(\mathbf{x}_{k+1}\right) - \mathbf{c}\left(\mathbf{x}_k\right), \cdots, \mathbf{c}\left(\mathbf{x}_{k+1}\right) - \mathbf{c}\left(\mathbf{x}_{\max(k+1-n,0)}\right)\right]$
  Solve $U_f \Sigma_f V_f{}^T = \Delta F$ with a singular value decomposition
  Solve $U_c \Sigma_c V_c{}^T = \Delta C$ with a singular value decomposition
  $\Delta F^{\dagger} = V_f \Sigma_f{}^{\dagger} U_f{}^T$
  $T_{k+1} = \Delta C \Delta F^{\dagger} + \left(I - U_c U_c{}^T\right)\left(I - U_f U_f{}^T\right)$
  if converged **then**
    break
  end if
end for

Fig. 1 The manifold mapping (MM) algorithm solving the optimization problem (7)

is reused, the mapping matrix T_k does not need to be initialized with the identity matrix at line 2, but can be determined with (17) (after the first time step).

The coarse optimization problem can be solved with a coupling scheme of the users choice. Here, the Anderson mixing method is employed to solve the coarse optimization problem. Note that the coupling scheme needs to meet the design specification $\mathbf{q}_k$, which can be included in the formulation of the residual for the FSI problem.

The mapping matrix T_k is of size $n \times n$ which can be prohibitively large for large scale applications. In order to reduce the memory requirements of the algorithm, the updated design specification $\mathbf{q}_k$ can be directly determined with only matrix vector multiplications such that the memory requirements do not exceed $n \times k$:

$$\begin{aligned} \mathbf{q}_k &= \mathbf{c}\left(\mathbf{x}_k\right) - T_k\left(\mathbf{f}\left(\mathbf{x}_k\right) - \mathbf{q}\right) \\ &= \mathbf{c}\left(\mathbf{x}_k\right) - \boldsymbol{\alpha} - \Delta C\left(\Delta F^{\dagger}\boldsymbol{\alpha}\right) + U_c\left[U_c^T\left(\boldsymbol{\alpha} - \boldsymbol{\beta}\right)\right] + \boldsymbol{\beta}, \end{aligned} \tag{20}$$

with $\boldsymbol{\alpha} = \mathbf{f}\left(\mathbf{x}_k\right) - \mathbf{q}$, and $\boldsymbol{\beta} = U_f\left(U_f^T\boldsymbol{\alpha}\right)$.

However, in case the simulation environment allows to store the mapping matrix T_k in memory, a secant update similar to the approach taken in [12] can be used:

$$T_k^{u+1} = T_k^u + \left(\Delta C - T_k^u \Delta F\right) \Delta F^{\dagger}, \tag{21}$$

where the pseudo inverse of ΔF can be computed as $\Delta F^{\dagger} = \left(\Delta F^T \Delta F\right)^{-1} \Delta F^T$ or via a singular value decomposition in the same manner as used by the original manifold mapping algorithm. The advantage of this approach is that the user does not need to specify the number of time steps the coupling scheme needs to reuse.

If the fluid and structure solvers are executed in serial, a separate synchronization step is necessary. Once the solution has been found by the fine model, the degrees of freedom of the coarse model need to be corrected [17]. Two different approaches can be applied. One approach is to restrict the data in the entire fluid and structure domain from the fine model to the coarse model. If such a system is not available since the used solvers are black box solvers, the interface traction and displacement calculated by the fine model can be applied to the fluid-structure interface of the coarse model, whereafter the flow equations and structure equations are solved by the coarse model. Note that this approach can result in a difference between the solution of the flow and structure domain after a certain number of time steps.

During the manifold mapping iterations, the same interface displacement is applied on the fine model and also on the coarse model. Therefore, only the coarse structural model needs to be synchronized with the fine model if the second synchronization approach is used. If the fine model and the coarse model use exactly the same structural model, the second approach will result in a perfectly synchronized coarse model.

In case the fluid and structure solvers are executed in parallel, however, the same interface displacement and interface traction is already applied on the fine model as

well as the coarse model. Therefore, a separate synchronization step is not necessary if the data in the entire fluid and structure domain is not restricted from the fine model to the coarse model.

4 Numerical Results

In this section the performance of the proposed acceleration algorithm for FSI is demonstrated for two test problems: two-dimensional incompressible laminar flow over a fixed cylinder with an attached flexible flap [43] and three-dimensional incompressible flow through a flexible tube [19]. We use foam-extend-3.1[1] for all simulations, a fork of the well-known OpenFOAM package.[2]

4.1 Fixed Cylinder with an Attached Flexible Flap

This test case, originally proposed in [43], consists of a two-dimensional incompressible laminar flow around a fixed cylinder with an attached flexible cantilever. In [43], three different scenarios are presented with different structure to fluid density ratios. For the results shown in this section, the unsteady fluid-structure interaction FSI3 case is selected. The structure to fluid density ratio is set to $\rho^s/\rho^f = 1$, resulting in a strong coupling between the fluid and the structure. The Reynolds number based on the diameter of the cylinder is 200. The reader is referred to [43] for further details on this benchmark problem.

The fluid domain and the structure domain are discretized with a second order finite volume method. A coupled solution algorithm [13] is employed instead of the well known PISO pressure-velocity coupling technique. Here, the continuity and the momentum equation are solved in a fully coupled implicit manner, instead of a segregated approach. A second order backward differencing scheme (BDF2) is used to integrate the governing equations in time. The fluid mesh is deformed with radial basis function interpolation [14]. The coarse model of the flow uses 1 457 cells. The grid is refined in each direction with a factor 4, resulting in 23 924 cells for the fine model of the fluid. The mesh of the structural model consists of 40 cells and is uniformly refined to form the fine mesh of the structure containing 328 cells. The relatively strict convergence criterion 10^{-5} is used for the fine model. The tolerance parameter of the coarse model is set to a stricter value 10^{-6}. A relative convergence measure is used for the fine as well as for the coarse model as in [11]. Pressure and velocity contours of the FSI3 benchmark are shown in Fig. 2.

[1] http://www.extend-project.de/.

[2] http://www.openfoam.org/.

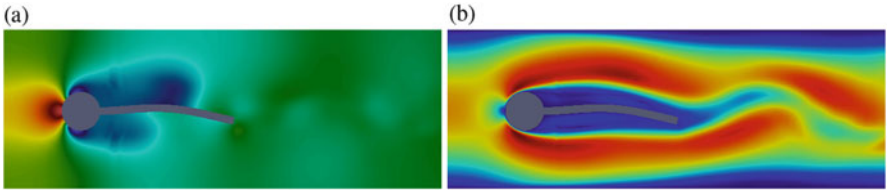

Fig. 2 Cylinder with an attached flap test case. Pressure and velocity contours of the FSI3 benchmark. (**a**) FSI3: pressure contours; (**b**) FSI3: velocity field

Table 1 Two dimensional flow over a fixed cylinder with an attached flexible flap FSI3. The influence of the reuse of information from previous time steps is studied for different coupling algorithms for the fluid-structure interaction problem. Manifold mapping (MM) is compared with the Anderson mixing method, and ML-IQN-ILS. Two different cases are considered, the flow and the structure solver are executed sequentially (S) or in parallel (P). The iteration numbers are averaged over the complete simulation

	Reuse 0		Reuse 8		Reuse 16		Reuse 24	
Method	n_f	n_c	n_f	n_c	n_f	n_c	n_f	n_c
S-Anderson	11.6	0.0	3.1	0.0	3.3	0.0	3.6	0.0
S-ML-IQN-ILS	8.9	13.5	3.3	4.3	3.7	4.5	3.7	4.6
S-MM	5.7	35.1	2.1	6.6	2.0	6.5	2.0	6.7
P-Anderson	26.3	0.0	5.7	0.0	5.7	0.0	8.1	0.0
P-ML-IQN-ILS	20.6	28.8	12.7	10.8	18.6	13.3	20.8	14.4
P-MM	11.2	150.6	3.4	29.4	3.0	32.9	2.9	34.7

Table 1 shows the averaged iteration numbers for the manifold mapping algorithm and also for the Anderson mixing method and ML-IQN-ILS. Reuse of information from previous time steps is considered in order to accelerate the convergence of the different coupling schemes. Sequential execution (S) of the fluid and structure solvers is compared with the parallel case (P).

In case the sequentially coupled manifold mapping technique (S-MM) is used and information from previous time steps is not included, approximately 5.7 fine model iterations are performed at every time step. The Anderson mixing method uses almost twice as many iterations per time step (11.6). With reuse of information from previous time steps, the least number of fine model iterations is 3.1 for the Anderson mixing method. However, this number increases in case information from more than 8 time steps is included. For the manifold mapping algorithm, the number of fine model iterations does not increase in case information from a large number of time steps is taken into account.

In case the fluid and the structure solver are executed in parallel, the number of fine model iterations increases to 11.2 for the manifold mapping technique. However, the Anderson mixing method uses 26.3 iterations per time step. In case information from previous time steps is reused by the different coupling algorithms, the number of fine model iterations decreases significantly. Again, it is important to not include information from a large number of time steps for the Anderson mixing

Table 2 Two dimensional flow over a fixed cylinder with an attached flexible flap FSI3. Manifold mapping (MM) is compared with the Anderson mixing method and ML-IQN-ILS. Two different cases are considered, the flow and structure solver are executed sequentially (S) or in parallel (P). The Jacobians of the different coupling algorithms are updated with the appropriate secant equation in order to take into account information from all previous time steps. The iteration numbers are averaged over the complete simulation

	Sequential		Parallel	
Method	n_f	n_c	n_f	n_c
Anderson	4.4	0.0	7.6	0.0
ML-IQN-ILS	4.8	5.4	8.2	8.5
MM	3.2	14.2	5.5	49.9

method, since the number of iterations increases from 5.7 (8 or 16 time steps reused) to 8.1 (24 time steps reused). For the manifold mapping algorithm, an increase in fine model iterations is not observed in case the information from an increasing number of time steps is reused.

The ML-IQN-ILS algorithm uses significantly less coarse model iterations in comparison to the manifold mapping technique due to the fact that the method optimizes the coarse model only once per time step, whereas for the manifold mapping algorithm the coarse model is optimized at every manifold mapping iteration. Note that in case the fluid and the structure are coupled in parallel, the number of fine model iterations is increased significantly compared to the staggered execution of the fluid and the structure solver.

Table 2 shows the averaged iteration numbers for the different coupling algorithms in case the Jacobians of the different coupling algorithms are updated with the appropriate secant equation in order to take into account information from all previous time steps. If we compare these results to those of Table 1, Table 1 shows worse performance if no time steps are reused, but better performance if the optimal number of time steps are reused.

4.2 Wave Propagation in a Three-Dimensional Elastic Tube

The second example simulates a wave propagating in a straight, three-dimensional elastic tube [8, 18, 27]. The geometry of the fluid and the structure domain is shown in Fig. 3. The length of the tube is 0.05 m. The tube has a thickness of 0.001 m. The inner diameter of the tube is 0.01 m. Both ends of the tube are fixed. Starting from $t = 0$ s until $t = 0.003$ s, the boundary condition for the gauge pressure at the inlet is set to the fixed value 1333.2 Pa. Thereafter, the inlet gauge pressure is set to zero. At the outlet, the pressure is fixed at zero at every time instant. The pressure contours at different time instants are shown in Fig. 4.

The fluid domain is governed by the incompressible Navier-Stokes equations. The flow has a density of 10^3 kg/m^3 and a dynamic viscosity of $3.0 \cdot 10^{-3}$ Pa $\cdot$ s.

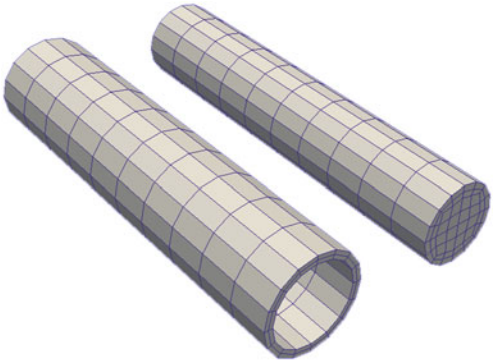

Fig. 3 Wave propagation in a straight elastic tube. The geometry and a very coarse mesh are shown for both the fluid and the structure domain

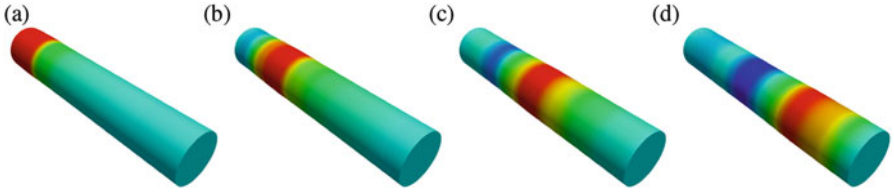

Fig. 4 Wave propagation in a straight tube. The pictures show pressure contours at different times on the fluid-structure interface. (**a**) $t = 0.0025\,\text{s}$; (**b**) $t = 0.0050\,\text{s}$; (**c**) $t = 0.0075\,\text{s}$ (**d**) $t = 0.0100\,\text{s}$

The structure is assumed to be elastic and compressible. The density of the elastic structure is $1.2 \cdot 10^3\,\text{kg/m}^3$, the Young's modulus is $3.0 \cdot 10^5\,\text{N/m}^2$, and the Poisson's ratio is 0.3.

The same solver as for the fixed cylinder with an attached flexible flap is used to simulate this problem. Thus, a finite volume solver based on a coupled solution algorithm is employed in combination with a second order time integration scheme. The coarse model of the fluid uses 2 600 cells and is refined in each direction with a factor 2, resulting in 20 800 cells for the fine model. Viscous effects are ignored for the coarse model of the fluid domain. Hence, the flow is governed by the incompressible Euler equations for the coarse model. The coarse model of the structure contains 800 cells and is also refined in each direction with a factor 2, resulting in a fine mesh with 6 400 cells. The initial solution of the displacement is determined with a state extrapolation from previous time steps for each numerical method under consideration.

Table 3 shows the averaged iteration numbers. The use of the manifold mapping algorithm reduces the number of fine model iterations from 15.6 for the Anderson mixing method to 6.3 in case the fluid and structure are executed in a sequential fashion and information from previous time steps is not considered. In case information from previous time steps is reused, the number of fine model iterations for the

Table 3 Three dimensional flow through a flexible tube. The influence of the reuse of information from previous time steps is studied for different coupling algorithms for the fluid-structure interaction problem. Manifold mapping (MM) is compared with the Anderson mixing method and ML-IQN-ILS. Two different cases are considered, the flow and the structure solver are executed sequentially (S), or in parallel (P). The iteration numbers are averaged over the complete simulation

	Reuse 0		Reuse 8		Reuse 16		Reuse 24	
Method	n_f	n_c	n_f	n_c	n_f	n_c	n_f	n_c
S-Anderson	15.6	0.0	5.9	0.0	5.1	0.0	4.9	0.0
S-ML-IQN-ILS	9.3	18.1	4.5	7.2	4.4	6.2	4.6	5.8
S-MM	6.3	51.0	3.4	17.6	3.4	15.7	3.3	15.4
P-Anderson	30.2	0.0	11.0	0.0	9.5	0.0	8.7	0.0
P-ML-IQN-ILS	14.6	34.0	7.6	12.2	7.0	10.2	6.9	9.3
P-MM	6.6	89.3	4.5	37.3	4.3	31.9	4.2	29.8

Table 4 Three dimensional flow through a flexible tube. Manifold mapping (MM) is compared with the Anderson mixing method, and ML-IQN-ILS. Two different cases are considered, the flow and the structure solver are executed sequentially (S), or in parallel (P). The Jacobians of the different coupling algorithms are updated with the appropriate secant equation in order to take into account information from all previous time steps. The iteration numbers are averaged over the complete simulation

	Sequential		Parallel	
Method	n_f	n_c	n_f	n_c
Anderson	6.8	0.0	11.7	0.0
ML-IQN-ILS	6.7	7.4	10.8	12.0
MM	4.6	28.5	5.8	44.5

Anderson mixing method reduces to 4.9, whereas the manifold mapping technique uses just 3.3 iterations per time step. The S-ML-IQN-ILS scheme outperforms the Anderson mixing method in terms of fine model iterations, though the manifold mapping technique is observed to use the least amount of fine model iterations.

When the fluid and structure solvers are coupled in parallel, the number of fine model iterations increases slightly to 6.6 for the manifold mapping technique, whereas the number of iterations for the Anderson mixing method is almost twice as high compared to the sequential coupling case. Including information from previous time steps accelerates the manifold mapping significantly to only 4.2 fine model iterations per time steps.

Table 4 shows the averaged iteration numbers for the same coupling algorithms in case the full Jacobians are updated with the appropriate secant equation in order to take into account the information from all previous time steps. Again, the sequential and the parallel coupling of the fluid and structure solvers is examined. The manifold mapping algorithm clearly outperforms the Anderson mixing method and the ML-IQN-ILS technique in terms of fine model iterations for both sequential and parallel cases. The number of fine model iterations increases with approximately one iteration for the parallel case compared to sequential coupling, whereas the ML-IQN-ILS and Anderson mixing technique use 3 and 4 extra iterations, respectively.

5 Conclusions

The use of the manifold mapping algorithm for partitioned fluid-structure interaction has been extended to the parallel coupling of the fluid and structure solvers. A coarse mesh can be selected for the low-fidelity model as well as an engineering model showing the flexibility of the manifold mapping algorithm. The method is non-intrusive in the sense that only input-output information of the high-fidelity and low-fidelity models is considered.

With numerical experiments, the potential of the coupling scheme is shown, comparing the performance of a serial execution of the fluid and structure solvers with a parallel coupling of the solvers. The number of fine model evaluations for a parallel coupled partitioned fluid-structure interaction simulations is reduced by approximately 55 %. With reuse of information from previous time steps, the algorithm is accelerated even further.

Acknowledgement The financial support of the Institute for Advanced Study (IAS) of the Technische Universität München, of SPPEXA, the German Science Foundation Priority Programme 1648—Software for Exascale Computing, and the Aerospace Engineering department at the Delft University of Technology is thankfully acknowledged.

References

1. Anderson, D.G.: Iterative procedures for nonlinear integral equations. J. ACM **12**(4), 547–560 (1965)
2. Badia, S., Quaini, A., Quarteroni, A.: Modular vs. non-modular preconditioners for fluid-structure systems with large added-mass effect. Comput. Methods Appl. Mech. Eng. **197**(49–50), 4216–4232 (2008)
3. Badia, S., Quaini, A., Quarteroni, A.: Splitting methods based on algebraic factorization for fluid-structure interaction. SIAM J. Sci. Comput. **30**(4), 1778–1805 (2008). DOI 10.1137/070680497. URL http://www.rmee.upc.es/homes/badia/articles/art015.pdf
4. Bandler, J.W., Biernacki, R.M., Chen, S.H., Grobelny, P.A., Hemmers, R.H.: Space mapping technique for electromagnetic optimization. IEEE Trans. Microwave Theory Tech. **42**, 2536–2544 (1994)
5. Bandler, J.W., Biernacki, R.M., Chen, S.H., Hemmers, R.H., Madsen, K.: Electromagnetic optimization exploiting aggressive space mapping. IEEE Trans. Microwave Theory Tech. **43**(12), 2874–2882 (1995)
6. Bandler, J.W., Cheng, Q.S., Dakroury, S.A., Mohamed, A.S., Bakr, M.H., Madsen, K., Søndergaard, J.: Space mapping: the state of the art. IEEE Trans. Microwave Theory Tech. **52**(1), 337–361 (2004)
7. Barker, A.T., Cai, X.C.: Scalable parallel methods for monolithic coupling in fluid–structure interaction with application to blood flow modeling. J. Comput. Phys. **229**(3), 642–659 (2010)
8. Bathe, K.J., Ledezma, G.A.: Benchmark problems for incompressible fluid flows with structural interactions. Comput. Struct. **85**(11–14), 628–644 (2007)
9. Bathe, K.J., Zhang, H.: A mesh adaptivity procedure for CFD and fluid-structure interactions. Comput. Struct. **87**(11–12), 604–617 (2009)

10. Blom, D.S., van Zuijlen, A.H., Bijl, H.: Acceleration of strongly coupled fluid-structure interaction with manifold mapping. In: Oñate, E., Oliver, X., Huerta, A. (eds.) Proceedings of the 11th World Congress on Computational Mechanics. 5th European Congress on Computational Mechanics. 6th European Congress on Computational Fluid Dynamics, pp. 4484–4495 (2014)
11. Blom, D.S., van Zuijlen, A.H., Bijl, H.: Multi-level acceleration with manifold mapping of strongly coupled fluid-structure interaction. Comput. Methods Appl. Mech. Eng. (2015)
12. Bogaers, A.E.J., Kok, S., Reddy, B.D., Franz, T.: Quasi-Newton methods for implicit black-box FSI coupling. Comput. Methods Appl. Mech. Eng. **279**, 113–132 (2014)
13. Darwish, M., Sraj, I., Moukalled, F.: A coupled finite volume solver for the solution of incompressible flows on unstructured grids. J. Comput. Phys. **228**(1), 180–201 (2009). DOI 10.1016/j.jcp.2008.08.027
14. de Boer, A., van Zuijlen, A.H., Bijl, H.: Radial Basis Functions for Interface Interpolation and Mesh Deformation. Lecture Notes in Computational Science and Engineering, vol. 71, Chap. 6, pp. 143–178. Springer, Berlin/Heidelberg (2010)
15. Degroote, J.: Partitioned simulation of fluid-structure interaction. Arch. Comput. Meth. Eng. **20**(3), 185–238 (2013)
16. Degroote, J., Vierendeels, J.: Multi-solver algorithms for the partitioned simulation of fluid-structure interaction. Comput. Methods Appl. Mech. Eng. **200**(25–28), 2195–2210 (2011)
17. Degroote, J., Vierendeels, J.: Multi-level quasi-Newton coupling algorithms for the partitioned simulation of fluid-structure interaction. Comput. Methods Appl. Mech. Eng. **225–228**, 14–27 (2012)
18. Degroote, J., Bruggeman, P., Haelterman, R., Vierendeels, J.: Stability of a coupling technique for partitioned solvers in FSI applications. Comput. Struct. **86**, 2224–2234 (2008)
19. Degroote, J., Bathe, K.J., Vierendeels, J.: Performance of a new partitioned procedure versus a monolithic procedure in fluid-structure interaction. Comput. Struct. **87**(11–12), 793–801 (2009)
20. Delinchant, B., Lahaye, D., Wurtz, F., Coulomb, J.L.: Manifold mapping optimization with or without true gradients. Math. Comput. Simul. **90**, 256–265 (2013)
21. Echeverría, D., Hemker, P.W.: Space mapping and defect correction. Comput. Methods Appl. Math. **5**(2), 107–136 (2005)
22. Echeverría, D., Hemker, P.W.: Manifold mapping: a two-level optimization technique. Comput. Vis. Sci. **11**(4–6), 193–206 (2008). DOI 10.1007/s00791-008-0096-y. URL http://dx.doi.org/10.1007/s00791-008-0096-y
23. Echeverría, D., Lahaye, D., Encica, L., Lomonova, E.A., Hemker, P.W., Vandenput, A.J.A.: Manifold-mapping optimization applied to linear actuator design. IEEE Trans. Magn. **42**(4), 1183–1186 (2006)
24. Fang, H.R., Saad, Y.: Two classes of multisecant methods for nonlinear acceleration. Numer. Linear Algebra Appl. **16**(3), 197–221 (2009)
25. Farhat, C., Lesoinne, M.: Two efficient staggered algorithms for the serial and parallel solution of three-dimensional nonlinear transient aeroelastic problems. Comput. Methods Appl. Mech. Eng. **182**(3–4), 499–515 (2000)
26. Felippa, C., Park, K., Farhat, C.: Partitioned analysis of coupled mechanical systems. Comput. Methods Appl. Mech. Eng. **190**(24–25), 3247–3270 (2001)
27. Fernández, M.Á., Moubachir, M.: A Newton method using exact jacobians for solving fluid-structure coupling. Comput. Struct. **83**(2–3), 127–142 (2005)
28. Ganine, V., Hills, N.J., Lapworth, B.L.: Nonlinear acceleration of coupled fluid-structure transient thermal problems by Anderson mixing. Int. J. Numer. Methods Fluids **71**(8), 939–959 (2013)
29. Gee, M., Küttler, U., Wall, W.: Truly monolithic algebraic multigrid for fluid-structure interaction. Int. J. Numer. Methods Eng. **85**(8), 987–1016 (2011). DOI 10.1002/nme.3001
30. Haelterman, R., Degroote, J., van Heule, D., Vierendeels, J.: The quasi-Newton least squares method: a new and fast secant method analyzed for linear systems. SIAM J. Numer. Anal. **47**(3), 2347–2368 (2009)

31. Haelterman, R., Degroote, J., van Heule, D., Vierendeels, J.: On the similarities between the quasi-Newton inverse least squares method and GMRes. SIAM J. Numer. Anal. **47**(6), 4660–4679 (2010)
32. Koziel, S., Bandler, J.W., Madsen, K.: Towards a regirous formulation of the space mapping technique for engineering design. In: IEEE International Symposium on Circuits and Systems, vol. 6, pp. 5605–5608. IEEE, New York (2005)
33. Küttler, U., Wall, W.A.: Fixed-point fluid–structure interaction solvers with dynamic relaxation. Comput. Mech. **43**(1), 61–72 (2008)
34. Küttler, U., Wall, W.A.: Vector extrapolation for strong coupling fluid-structure interaction solvers. J. Appl. Mech. **76**(2), 021205 (2009)
35. Marklund, P.O., Nilsson, L.: Simulation of airbag inflation processes using a coupled fluid structure approach. Comput. Mech. **29**(4–5), 289–297 (2002)
36. Mehl, M., Uekermann, B., Bijl, H., Blom, D.S., Gatzhammer, B., van Zuijlen, A.H.: Parallel coupling numerics for partitioned fluid-structure interaction simulations. Comput. Math. Appl. (2015)
37. Michler, C., van Brummelen, E.H., de Borst, R.: An interface Newton–Krylov solver for fluid–structure interaction. Int. J. Numer. Methods Fluids **47**(10–11), 1189–1195 (2005)
38. Michler, C., van Brummelen, H., de Borst, R.: An investigation of Interface-GMRES(R) for fluid–structure interaction problems with flutter and divergence. Comput. Mech. **47**(1), 17–29 (2011)
39. Ross, M.R., Felippa, C.A., Park, K., Sprague, M.A.: Treatment of acoustic fluid-structure interaction by localized Lagrange multipliers: formulation. Comput. Methods Appl. Mech. Eng. **197**(33–40), 3057–3079 (2008). DOI 10.1016/j.cma.2008.02.017. URL http://linkinghub.elsevier.com/retrieve/pii/S0045782508000625
40. Scholcz, T.P., van Zuijlen, A.H., Bijl, H.: Space-mapping in fluid-structure interaction problems. Comput. Methods Appl. Mech. Eng. **281**, 162–183 (2014)
41. Stein, K., Benney, R., Kalro, V., Tezduyar, T.E., Leonard, J., Accorsi, M.: Parachute fluid-structure interactions: 3-D computation. Comput. Methods Appl. Mech. Eng. **190**(3–4), 373–386 (2000)
42. Tezduyar, T.E., Sathe, S., Keedy, R., Stein, K.: Space–time finite element techniques for computation of fluid–structure interactions. Comput. Methods Appl. Mech. Eng. **195**(17), 2002–2027 (2006)
43. Turek, S., Hron, J.: Proposal for numerical benchmarking of fluid-structure interaction between an elastic object and laminar incompressible flow. In: Bungartz, H.J., Schäfer, M. (eds.) Fluid-Structure Interaction: Modelling, Simulation, Optimisation, vol. 53, pp. 371–385. Springer, Berlin/Heidelberg (2006)
44. Uekermann, B., Bungartz, H.J., Gatzhammer, B., Mehl, M.: A parallel, black-box coupling algorithm for fluid-structure interaction. In: Proceedings of 5th International Conference on Computational Methods for Coupled Problems in Science and Engineering, pp. 1–12. Ibiza (2013)
45. van Brummelen, E.H.: Partitioned iterative solution methods for fluid-structure interaction. Int. J. Numer. Methods Fluids **65**(1–3), 3–27 (2011)
46. van Zuijlen, A.H., Bijl, H.: Multi-Level Accelerated Sub-Iterations for Fluid-Structure Interaction. *Lecture Notes in Computational Science and Engineering*, vol. 73, Chap. 1, pp. 1–25. Springer, Berlin/Heidelberg (2010)
47. Walker, H.F., Ni, P.: Anderson acceleration for fixed-point iterations. SIAM J. Numer. Anal. **49**(4), 1715–1735 (2011)